Available online at www.sciencedirect.com
ScienceDirect
International Journal of Mass Spectrometry 260 (2007) 146–157
International Journal of Mass Spectrometry
www.elsevier.com/locate/ijms

Mass spectral analysis and imaging of tissue by ToF-SIMS—The role of buckminsterfullerene, C_{60}^+, primary ions

Emrys A. Jones *, Nicholas P. Lockyer, John C. Vickerman

Surface Analysis Research Centre, Centre for Instrumentation and Analytical Science, School of Chemical Engineering and Analytical Science, The University of Manchester, UK

Received 23 June 2006; received in revised form 1 September 2006; accepted 8 September 2006
Available online 9 October 2006

Abstract

Recent developments in desorption/ionisation mass spectrometry techniques have made their application to biological analysis a realistic and successful proposition. Developments in primary ion source technology, mainly through the advent of polyatomic ion beams, have meant that the technique of secondary ion mass spectrometry (SIMS) can now access the depths of information required to allow biological imaging to be a viable option.

Here the role of the primary ion C_{60}^+ is assessed with regard to molecular imaging of lipids and pharmaceuticals within tissue sections. High secondary ion yields and low surface damage accumulation are demonstrated on both model and real biological samples, indicating the high secondary ion efficiency afforded to the analyst by this primary ion when compared to other cluster ion beams used in imaging. The newly developed 40 keV C_{60}^+ ion source allows the beam to be focused such that high resolution imaging is demonstrated on a tissue sample, and the greater yields allow the molecular signal from the drug raclopride to be imaged within tissue section following in vivo dosing.

The localisation shown for this drug alludes to issues regarding the chemical environment affecting the ionisation probability of the molecule; the importance of this effect is demonstrated with model systems and the possibility of using laser post-ionisation as a method for reducing this consequence of bio-sample complexity is demonstrated and discussed.

Keywords: C_{60}^+; Tissue imaging; Matrix effects; Pharmaceutical

1. Introduction

Detailed chemical characterisation of complex biological systems with good spatial resolution, be they simple cells or complex tissues, is the holy grail for many analytical scientists applying their techniques to biology. At first sight mass spectrometry seems to provide all the component capabilities to provide what is needed. It has tremendous chemical specificity via mass spectral fragmentation patterns, accurate mass measurement and the tandem MS techniques and there is an enormous knowledge bank in biological mass spectrometry to resort to, to facilitate data interpretation. Spatially resolved MS analysis is increasingly on offer, and one of these techniques, secondary ion mass spectrometry (SIMS), has for many years been able to provide sub-micron spatial resolution using liquid metal ion beams such as Ga^+ or In^+. Levi-Setti's group in Chicago have shown that very high primary beam energies are able to offer sub-50 nm resolution [1]. This application has very successfully probed specific local chemistry through small fragments, e.g., CN^-, or atomic secondary ions, frequently using isotope enrichment techniques [2–4]. However, analysts and biological scientists aspire to unravelling the molecular complexity of the systems under study by exploiting the MS capability of identifying molecular ions or large chemically characteristic fragment ions. Matrix assisted laser desorption/ionisation's (MALDI) well-known ability to provide this capability for many classes of bio-molecules has driven the development of spatially resolved MALDI [5,6]. Impressive progress has been made such that routine imaging can provide spatial resolution down to ~10 μm [7]. There are a number of issues that provide further challenges such as matrix crystal size and dispersion [8], power thresholds for ion generation as laser spot size decreases [9], etc. Nevertheless, the prospects look good.

* Corresponding author. Tel.: +44 161 3062727; fax: +44 161 3069321.
E-mail address: emrys.jones@manchester.ac.uk (E.A. Jones).

1387-3806/$ – see front matter © 2006 Elsevier B.V. All rights reserved.
doi:10.1016/j.ijms.2006.09.015

The introduction of polyatomic primary ion beams into SIMS has provided a substantial leap in the capability of SIMS to access bio-molecules with good sensitivity. The extremely low secondary ionisation probability ($\leq 10^{-4}$, similar for MALDI) [10] coupled with the high surface sensitivity (nm) provided a severe limitation on realistic molecular SIMS analysis below 1 μm spatial resolution. There are just too few molecules in the sampling volume to deliver an adequate yield for proper analysis when using atomic primary ions. The liquid metal ion beams using gold and bismuth deliver good quantities of cluster ions M_n^+, where $n = 1$–5 [11,12]. Such ions greatly increase the secondary ion yield of molecular species in the *m*/*z* range 400–3000 [11–13]. Although this seems mainly to be a consequence of increased sputter yield, it has pushed the spatial resolution attainable for high ion yield molecular ions below 1 μm. However, attainable spatial resolution in SIMS is also limited by the fact that the primary ions generate bombardment-induced chemical damage. Although the analyte ions are derived from the topmost atomic layers, kiloelectronvolt atomic and cluster projectiles penetrate some tens of nanometers into the sample with concomitant sub-surface chemical damage. After successive impacts in the same region the analyte ions reflect this accumulated chemical damage and are no longer representative of the original material. This phenomenon limits the number of useful ions accessible from a given pixel area, and gave rise to the so-called *static limit*—the primary ion dose beyond which the secondary ions detected were increasingly likely to be unrepresentative of the original chemistry.

It has been shown that molecular primary ions such as SF_5^+ and more recently C_{60}^+ not only deliver very large increases in yields of mid-sized molecular and fragment ions, in many cases they show much smaller, even zero, damage cross-sections [14–16]. These phenomena are thought to result from multiple low energy (<keV) impacts due to the fragmentation of the incident polyatomic ion. The low damage cross-section is thought to result from the combination of very high sputter yield from the surface and much-reduced penetration depth [17,18]. Essentially the chemical damage arising from each impact is largely contained within the ejected volume. Potentially this means that the static limit can be ignored and yields per pixel could enable useful spatially resolved molecular analysis in the ∼100 nm region. The fact that with many systems there is no evidence that chemical damage accumulates, also means that molecular depth profiling becomes possible, enabling analysis in three dimensions. In practical terms, these molecular ion beams are less easy to focus than the liquid metal ion beams, but 200 nm is accessible [19] and for ultimate spatial resolution a combination of C_{60}^+ and a liquid metal cluster may be a useful compromise in some cases. Thus, it would seem the use of ion beams such as C_{60}^+ could provide an analytical overlap with MALDI. It is not likely that SIMS will be able to match MALDI's capability in protein analysis, but spatially resolved analysis of smaller molecules is likely to be the strength of SIMS.

However, whilst SIMS using molecular ion beams has great potential, there are other challenges. SIMS is a vacuum technique and whilst in contrast to the new atmospheric MS methods – DESI [20] and ELDI [21] – this facilitates the provision of high spatial resolution ion beams, it complicates the sample handling of biological samples. The majority of biological samples analysed by ToF-SIMS, including cells and tissues, have been freeze-dried and a number of the diagnostic ions observed from these systems have been assigned to lipids, including cholesterol, sulphatides, phosphatidylinositols, phosphatidylcholines, etc., demonstrating that these species remain localised and amenable to analysis using this methodology [22].

The other major challenge is the *matrix effect*. This effect can complicate all mass spectrometry techniques [23]. Within SIMS the effect has been known for many years, the ionisation probability of a given element varying greatly depending upon the composition of its immediate environment [10]. This concept of ionisation probability being dependant upon the chemical environment has been exploited by the desorption MS techniques fast atom bombardment (FAB) and MALDI, where the analyte is incorporated into an excess of a suitable matrix. In the case of FAB this is typically a liquid such as glycerol, in MALDI the analyte is typically co-crystallised onto the target plate with an excess of an organic acid molecule. Although mainly used for the analysis of isolated species, the use of MALDI for MS imaging has become a rapidly expanding application, however, great care must be taken with the application of matrix to the sample surface in order to obtain accurate results. A major benefit of cluster ion sources for SIMS analysis is that they offer secondary ion yield enhancements without the need for chemical modification of the surface, unlike the techniques mentioned here. However, the matrix effect can be just as important when analysing samples in an unaltered state, as one compound may strongly influence the detection of another that it is co-localised with. An understanding of the matrix effect with respect to organic molecules is essential to allow the results obtained to be interpreted correctly.

This paper reports on some recent investigations into the contribution the use of C_{60}^+ primary ions can make in biological analysis and imaging. The data presented here are largely based on rat brain sections, a tissue sample that has become de rigour in these proving studies, with accompanying data from standard samples of biologically significant model systems.

2. Experimental

2.1. Materials

2.1.1. Model system samples

All compounds were purchased from Sigma–Aldrich (Poole, UK) and used without further purification. For the lipid depth profiling experiments, films of the pure compounds were created by spin casting the lipid onto a cleaned silicon wafer (Agar, Stansted, UK) from a 1×10^{-2} M trichloromethane solution. Rat brain homogenate was supplied by GlaxoSmithKline (Harlow, UK) and was a 50:50 mixture with deionised water; the sample was stored at −20 °C until required. Following thawing an aliquot was taken and spiked with a 1×10^{-2} M aqueous solution of the drug molecule such that the drug concentration was 1% (w/w) based on wet weight. A thin film was created on silicon wafers by drawing 10 μL of the mixture across the wafer with the edge of a glass pipette.

To layer a thin film of drug onto the control tissue section, 5 μL of a 1×10^{-3} M solution of haloperidol in trichloromethane was spun cast. The drug and lipid mixtures were prepared from trichloromethane solutions of cholesterol, dipalmatoylphosphatidylcholine (DPPC) and atropine mixed together to yield 1:1 molar ratios of the drug to lipid. These mixtures were then spun cast onto silicon substrates.

2.1.2. Tissue sections

The rat brain sections were supplied by GlaxoSmithKline. After collection, the brains were snap frozen in liquid nitrogen then cryo-microtomed, with the 12 μm sections being mounted on cleaned stainless steel segments. The sections were stored at −80 °C until analysis. Prior to introduction into the instrument, the samples were brought to room temperature in a desiccator for 2 h. For the sections from the raclopride in vivo drug study, 250–350 g male rats received a constant rate infusion of a 0.5 mg/mL solution administered at a target dose rate of 1.5 mg/kg/h for 6 h.

2.2. ToF-SIMS

All ToF-SIMS analyses performed in the studies reported here were carried out using a *Bio-ToF-SIMS* instrument, the design of which has been described elsewhere [24]. The instrument is equipped with both a C_{60}^+ and a Au_n^+ ion source. The data presented here were acquired with the sources set up so that the 40 kV Wien filtered C_{60}^+ ion gun (Ionoptika Ltd., UK) [25] delivered 200 pA into a 1 μm diameter spot; the 25 kV Wien filtered LMIG (Ionoptika Ltd.) [26], provided Au^+ and Au_3^+ at 1 nA and 100 pA currents, respectively, with spot sizes in the region of 500 nm diameter.

The sample was held at ground potential during ion impact. Secondary ions were directed into a two-stage reflectron ToF-MS by applying a delayed extraction pulse of 2.5 kV. Ions were post-accelerated to 20 keV and detected using a dual microchannel plate assembly. Unless otherwise stated, flight times were recorded on a 1 ns time-to-digital converter (Fast Comtec GmbH). Charge compensation during analysis is performed by pulsing low energy (25 eV) electrons onto the sample between successive primary ion pulses. During the depth profiling experiments the field of view for the etching was four times larger than the area used for analysis in order to avoid crater-edge effects. During etching a dc low energy (25 eV) electron beam is used to offset sample charging. With the exception of experiments where large primary ion doses are intentionally used, all spectra and images were acquired with ion doses below 1×10^{12} ions/cm^2, and the electron dose was kept below 1×10^{18} electrons/m^2. The SIMS analyses of pure films were carried out in triplicate in order to minimise the effect of spot-to-spot heterogeneity. For the tissue section yield determinations, three separate samples were analysed on different days with three different areas of the corpus callosum of each being analysed. The reported values are the average of all relevant analyses, the relative standard deviation of the results obtained was less than 10% in all cases.

For the larger scale tissue section imaging, composite images are built up from numerous separate analyses typically of 600 μm × 600 μm areas, with the sample moved accurately between each analysis using precision micrometers.

Laser post-ionisation was carried out using a SL312 Nd:YAG laser (EKSPLA Ltd., Lithuania). This system provides 150 ps pulses using backward stimulated Brillouin scattering. Post-ionisation was performed using 5 mJ, 266 nm laser pulses, focused with a 40 cm fused-silica lens. The ion gun pulse width was extended to 2 μs for these experiments and the sample was cooled to ∼150 K to eliminate the contribution of gas phase drug species to the post-ionisation signal. To avoid saturation effects, a 2 ns time resolution transient recorder (PDA500, Signatec, USA) was used to record signals from post-ionisation and corresponding SIMS experiments.

3. Results and discussion

3.1. C_{60}^+ primary ions for biological analysis

It has been clear for many years that cluster ion bombardment can provide excellent secondary ion per primary ion yields from organic surfaces. This advantageous feature has been applied to biological sample in many ways, one being mapping of lipids in tissue sections. Work with metal clusters such as Au_n^+ [22,25] and Bi_n^+ [13,26] have allowed a new level of molecular information to be extracted from tissue sections under SIMS analysis without the need for surface modification such as matrix addition [27] or gold deposition [28], which have also been shown to significantly increase secondary ion signal. Both have demonstrated that the distribution of lipids can be determined based on characteristic fragments and in some cases the molecular ions, allowing the unique distribution of phosphoglycerides, cholesterol and sphingolipids to be mapped within the section.

Yield enhancements of up to three orders of magnitude have been reported for the polyatomic primary ion C_{60}^+ over gallium [29] for standard samples of biologically relevant lipids such as phospholipids. With these encouraging results in mind, comparative analysis of tissue sections have been carried out to determine whether these advantageous effects are also experienced in the more complex, 'real world' sample types. Shown in Fig. 1 are positive ion spectra acquired with 25 keV Au^+ and 40 keV C_{60}^+ primary ions from the same white matter domain of a rat brain section.

The spectra presented clearly show the increase in molecular information obtained from biological tissue that is provided by the use of C_{60}^+ over the monoatomic Au^+ beam. Even though the primary ion dose used for the collection of the C_{60}^+ spectrum was 20 times less than used for the Au^+ spectrum the intensity of the peaks relating to cholesterol (*m/z* 369 and 385) and the phospholipids (*m/z* 700–800) are an order of magnitude greater. This significant yield enhancement allows for greater molecular information to be obtained for a given primary ion dose; however, the total obtainable signal from a given area will depend upon the disappearance cross-section of the various beams. If the yield enhancement is coupled to a greater rate of molec-

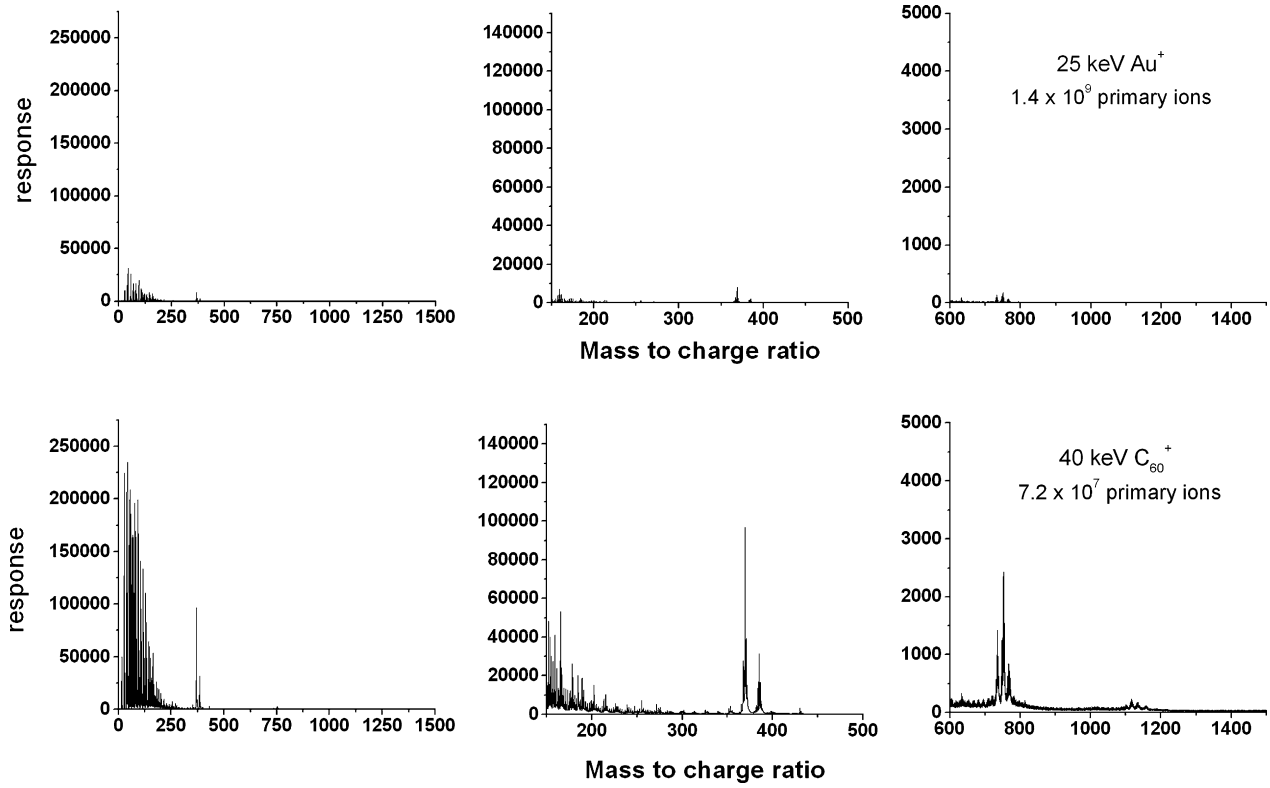

Fig. 1. Comparison of monoatomic Au^+ and polyatomic C_{60}^+ ion beams for the collection of molecular information from a section of rat brain. The ion doses used are quoted on the spectra. The major molecular peaks are those from cholesterol in the *m/z* 360–390 region, molecular ions from phospholipids in the region *m/z* 700–800 and their dimers in the group above *m/z* 1100.

ular signal decay, then the overall efficiency of secondary ion generation may not be significantly enhanced.

The stability of molecular signal from a surface under C_{60}^+ bombardment was initially investigated for lipids typically found within animal tissue; the first to be presented here is cholesterol, which is abundant within the membranes of cells. The plots in Fig. 2 show the behaviour of the quasi-molecular ions at *m/z* 369 $[M+H-H_2O]^+$, and *m/z* 385 $[M-H]^+$ from a pure film of cholesterol spun cast onto silicon which is subjected to increasing primary ion doses from three beams, Au^+, Au_3^+ and C_{60}^+ all at 15 keV. For C_{60}^+, the secondary ion intensity from both the quasi-molecular ions, *m/z* 369 and 385, reach a steady state near that of the initial value, whilst with the Au^+ and Au_3^+ beams the molecular signal is lost to the baseline noise by 4×10^{13} ions/cm^2. Although the secondary ion yields per primary ion of the Au_3^+ and C_{60}^+ are comparable, there is an obvious difference in the chemical damage caused to the surface during the impact. This experimental finding is supported by the molecular dynamic simulations carried out by the Garrison group at Penn State, where, in an amorphous ice layer, the energy from an Au_3^+ impact is deposited to much deeper depths than C_{60}^+ [30], thus affecting the sub-surface species more severely resulting in the accumulation of beam-induced chemical damage. It is the significant disappearance cross-section that

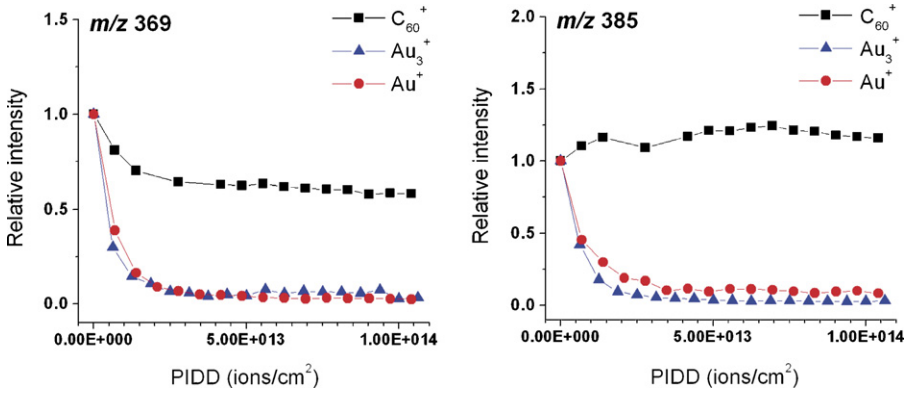

Fig. 2. A comparison of the stability of quasi-molecular ion intensity from a cholesterol film under prolonged bombardment by Au^+, Au_3^+ and C_{60}^+ primary ion beams all at 15 keV. The plots show the relative peak intensity for the $[M+H-H_2O]^+$ ion at *m/z* 369 and the $[M-H]^+$ ion at *m/z* 385 with respect to primary ion dose.

reflects this bombardment-induced damage that greatly reduces the potential of Au_3^+ and other LMIG cluster ions for the high spatial resolution analysis of biological systems.

Another abundant lipid within tissue, as well as being a well-studied molecule with the SIMS technique is dipalmatoylphosphatidylcholine. The data presented in Fig. 3 show the accumulated signal intensity of the *m/z* 184 ion, the phosphatidylcholine (PC) headgroup, from a pure DPPC film, plotted as a function of primary ion dose for both Au^+ and C_{60}^+ analysis. Due to the low damage accumulation that occurs following the C_{60}^+ impact, the surface under analysis continues to yield characteristic ion fragments even following an ion dose of 1×10^{15} ions/cm^2. This is in direct contrast to the monoatomic Au^+ where surface damage accumulation creates a boundary value beyond which very little molecular information is obtained, as is clearly illustrated in Fig. 3. There are therefore different limits to the amount of molecular information that can be obtained from a given area. Au and Au_3^+ analyses are restricted by the rate at which the surface species are damaged, whilst the amount of secondary ion signal that can be collected during a C_{60}^+ analysis is restricted only by the availability of the molecular species within the volume of analysis and the time taken to collect the data. As shown is Fig. 3, the initial yield enhancement for C_{60}^+ over the Au^+ is a factor of 60 (note different *y*-axis scale), however, following an ion dose of 1×10^{15} ions/cm^2 the C_{60}^+ analysis has yielded approximately 3500 times more of the characteristic molecular ion.

The data presented in Figs. 1 and 3 are comparisons between the Au^+ primary ion and C_{60}^+, in order to demonstrate the benefit of C_{60}^+ analysis over the monoatomic primary ion beam. However, an important feature of liquid metal ion source is the presence of cluster ions within the primary ion beam. The cluster most commonly used with the Au:Ge source is Au_3^+, the non-linear yield enhancements it delivers have been previously reported [11]. Nevertheless, as was demonstrated in Fig. 2, the rate of molecular signal disappearance under Au_3^+ bombardment is very different to the steady state that occurs when C_{60}^+ is used.

Table 1
The comparison of secondary ion yield and disappearance cross-section values for the $[M-H]^+$ ion of cholesterol at *m/z* 385 using Au^+ and Au_3^+ primary ion beams, from a pure film of cholesterol on silicon

	Secondary ion per primary ion, Y (*m/z* 385)	Disappearance cross-section, σ (cm^2)	Efficiency, E (cm^{-2})
Au^+	5.5×10^{-6}	4.5×10^{-14}	1.2×10^8
Au_3^+	6.5×10^{-5}	7.3×10^{-14}	9.0×10^8
Au_3^+/Au^+	12	2	7

From these values, the secondary ion generation efficiency is calculated.

In order to asses the potential of the cluster ion Au_3^+ for biological imaging, yield (Y) and disappearance cross-section data (σ) were collected for both Au^+ and Au_3^+ from various areas of a spun cast film of cholesterol on silicon. These data are presented in Table 1. The ion that is used to calculate the data is the $[M-H]^+$ ion of cholesterol at *m/z* 385. The disappearance cross-section, $\sigma(X_i^+)$, is calculated by obtaining the gradient of the decrease in the intensity of this ion, $N(X_i^+)$, with increasing ion dose density (PIDD) when plotted on a natural log scale.

$$N(X_i^+) = N(X_i^+)_{t=0} \exp(-\sigma(X_i^+)\,\mathrm{PIDD}) \quad (1)$$

From the yield and disappearance data the efficiency of secondary ion generation can be calculated.

$$E(X_i^+) = \frac{Y(X_i^+)}{\sigma(X_i^+)} \quad (2)$$

When these efficiencies are compared, it is clear that there is an advantage in using Au_3^+ rather than Au^+, however, as the rate of

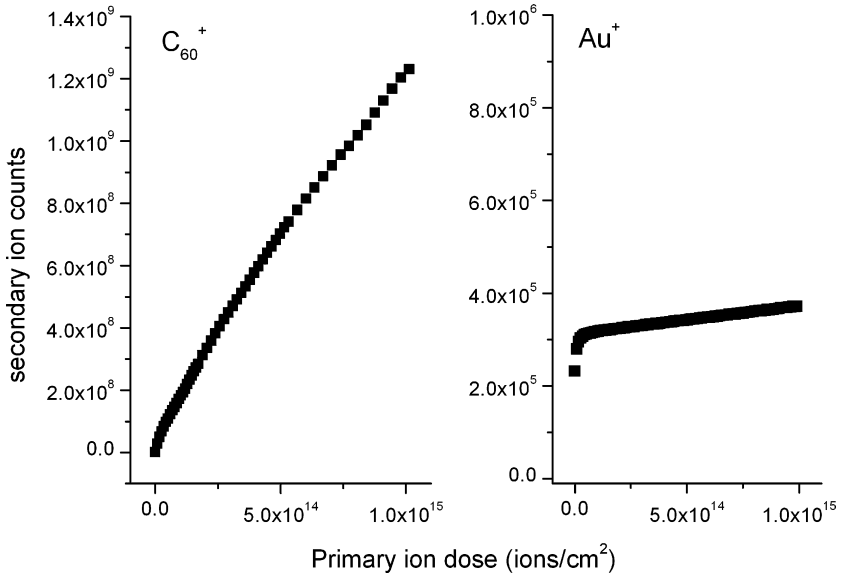

Fig. 3. Accumulated secondary ion counts for the peak *m/z* 184 from a pure film of DPPC with C_{60}^+ and Au^+ primary ion beams, based on data taken from damage profiles acquired at 15 keV. The accumulation of surface damage limits the useful signal that is obtainable from a given area under Au^+ bombardment, which is not the case with C_{60}^+.

molecular signal decay is greater with the cluster ion beam, this limits the potential advantage of this beam. Conversely, the high yields and in particular the low damage accumulation effects provided by the C_{60}^+ are encouraging, nevertheless, it needs to be demonstrated that these results carry through into real world samples.

To determine whether this is the case, a similar study was carried out on the rat brain tissue to determine the efficiencies of secondary ion formation of the $[M-H]^+$ ion of cholesterol from the corpus callosum, with the values for Au^+ being compared to that of the C_{60}^+ for a number of areas within this region of the tissue. As can be observed from the data presented in Table 2, the efficiency of the secondary ion formation and detection with C_{60}^+ is approximately 180 times greater than that from the Au^+. In order to compare this performance to that of other primary ion sources, data are taken from work on a similar sample by Brunelle and co-workers [13], and presented in the same table (denoted by an asterisk). As an experimental comparison between C_{60}^+ and bismuth ion sources on the same sample and on the same instrument was not possible, we have attempted to cross-standardise our data with that from ref. [13] using yields obtained using the Au^+ primary ion. The yield from an Au^+ (197 Da) and Bi^+ (209 Da) impact at the same energy should be comparable [13]. Thus, spectra were collected with the Au^+ ion source at 25 keV with the aim of directly comparing it to the 25 keV Bi^+ yields from ref. [13]. Although the bismuth yield is six times greater than that obtained for the Au^+, the efficiency values for the Au^+ on the Bio-ToF-SIMS and the Bi^+ reported are very similar. This would support the argument of parity between the two projectiles, and validate the comparison between the bismuth ions and C_{60}^+.

From these data, it is evident that due to the low damage accumulation experienced with the C_{60}^+ source, it significantly outperforms the other cluster ion sources with regard to detection efficiency. It is a factor 200 higher than the atomic primary ions and ~30 times the LMIG cluster ions. It is notable that Bi_3^+ is only five times more efficient than Au^+ and Bi^+. Thus, although there are yield benefits compared to Au^+ and Bi^+ from using the LMIG cluster ions, the damage cross-sections are still significant and, despite their small spot size capability, this will limit the minimum pixel area that can be usefully sampled. The value for the disappearance cross-section for the C_{60}^+ in Table 2 is the average taken across a primary ion dose of 1×10^{14} ions/cm^2. However, as shown in Fig. 2, the decrease of molecular signal from a surface under C_{60}^+ for most systems cannot be fitted to an exponential decay curve, and a steady state is reached at a point where there is still significant molecular signal. If the disappearance cross-section was calculated within this steady state then the value nears 3×10^{-15} cm^2, which would further increase the efficiency. These data clearly demonstrates the advantages of using polyatomic primary ions such as C_{60}^+ as projectiles for SIMS analysis of biological samples.

3.2. Drug molecules within brain homogenate

One area within which imaging mass spectrometry promises exciting new possibilities is drug discovery, especially as a replacement or complementary technique to autoradiography and fluorescence microscopy for mapping the location of drugs within tissue sections. However, these pharmaceutical compounds will be at a much lower surface abundance than the native compounds that have been imaged in the past with SIMS. It may be the case that there are too few drug molecules within the upper monolayers to yield a detectable signal from the sample.

It is in cases such as this that the low damage accumulation seen with the polyatomic species will be significant. Although there are many examples that demonstrate very low or even zero damage accumulation under C_{60}^+ primary ion bombardment, it is important to determine whether the presence of a complex matrix could hinder such effects. The model systems that are presented here, haloperidol and ipratropium bromide within brain homogenate, are very challenging samples, the brain homogenate being a complex mix of proteins and lipids, as well as containing high levels of salts.

From the plots in Fig. 4 it is evident that as with the previous examples, following an initial change in signal intensity a steady state is reached for the quasi-molecular ion species of the molecules under analysis. In Fig. 4, which shows the behaviour of the brain homogenate spiked with the drug haloperidol, there is a significant increase in the intensity of the $[M+H]^+$ ion for the drug following the initial sputtering. It could be concluded that the drug is being uncovered from beneath a layer of phospholipid that would have segregated to the surface of the aqueous suspension due to its hydrophobic tail groups. This is supported by the disappearance of the characteristic ion for the phospholipid phosphatidylcholine headgroup. Although this rapid decrease in signal from the PC headgroup is also seen in the second system, that of the brain homogenate spiked with ipratropium bromide, the quasi-molecular ion of the drug does not increase, whereas

Table 2
Performance comparison of different ions beams for the detection of the $[M-H]^+$ ion of cholesterol (m/z 385) from the corpus callosum region of a section of rat brain

Primary ion	Projectile mass	Projectile energy (keV)	Secondary ion per primary ion, Y (m/z 385)	Disappearance cross-section, σ (cm^2)	Efficiency, E (cm^{-2})
Au^+	197	25	1.5×10^{-5}	4.0×10^{-14}	3.8×10^{8}
$^*Bi^+$	209	25	8.4×10^{-5}	2.8×10^{-13}	3.0×10^{8}
$^*Bi^{3+}$	627	25	7.1×10^{-4}	4.2×10^{-13}	1.7×10^{9}
$^*Bi_5^{2+}$	1045	50	9.9×10^{-4}	3.5×10^{-13}	2.8×10^{9}
C_{60}	720	40	1.4×10^{-3}	2.0×10^{-14}	7.0×10^{10}

The data marked with an asterisk were taken from ref. [13], and were acquired on a different instrument and sample.

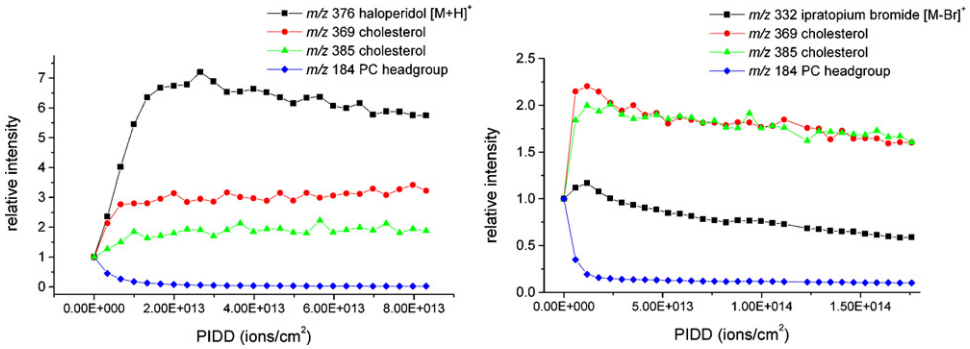

Fig. 4. Depth profiles of mixtures of brain homogenate and two drug molecules, haloperidol and ipratropium bromide, using 20 keV C_{60}^+ primary ion beam. The plots demonstrate the behaviour of the quasi-molecular ion of the drug as well as ions relating to cholesterol and the phosphatidylcholine headgroup.

the ions for the cholesterol do. The difference in the behaviour of ipratropium bromide to that of the haloperidol may be due to a more homogeneous distribution of the drug within the mixture, so that the concentration at the surface is representative of the bulk. Another possible explanation is that chemical modification of the surface, in this case the disappearance of the phospholipids, following C_{60}^+ bombardment has created a more favourable chemical environment for the creation of $[M+H]^+$ ions, leading to the large increase in signal from the haloperidol. As the ipratropium bromide quasi-molecular ion is formed by the dissociation of the molecular fragment from the bromide counter ion, changes in the chemical environment should not affect the detection of this species, which is illustrated in Fig. 4. The salient point from both analyses is that the molecular ion signal from a drug species within a biological matrix does not deteriorate with prolonged C_{60}^+ bombardment. This alludes to the possibility that molecular information can be extracted not only from the immediate surface of a sample, as in the traditional static SIMS approach, but instead by the removal of numerous monolayers increasing the number of drug molecules available for sampling, thus improving the probability that the molecule will be detected.

3.3. Tissue imaging

In order to obtain accurate information about the distribution of compounds within a biological sample, good detection limits should be coupled to high spatial resolution. In Section 1, it was mentioned that polyatomic ion beams are now being developed with spot sizes that are approaching those of the monoatomic

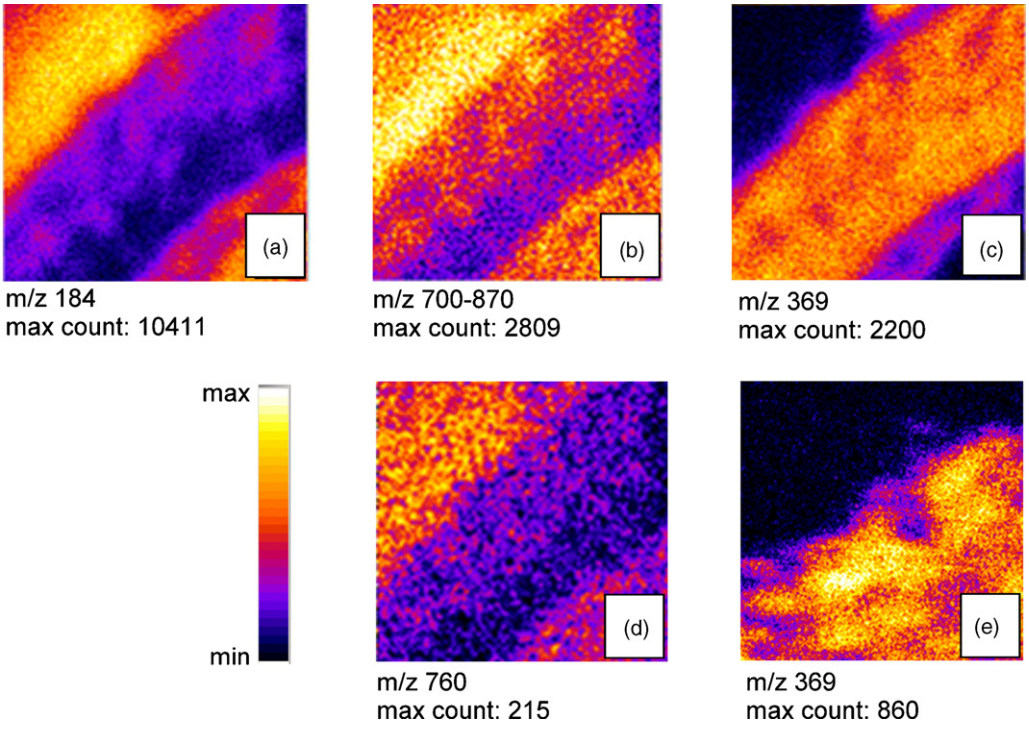

Fig. 5. Selected ion images from a 40 keV C_{60}^+ analysis of an area of rat brain tissue incorporating part of the corpus callosum. Images (a–d) are of a 800 μm × 800 μm area, the total primary ion dose was 4.3×10^{11} ions/cm^2, the maximum count in a pixel within the images are quoted. The images show the distribution of: (a) PC headgroup (*m/z* 184), (b) the collection of lipid peaks in the mass range 700–850, (c) cholesterol (*m/z* 369) and (d) a single phospholipid–PC 34:1 (*m/z* 760). Image (e) is from a 200 μm × 200 μm field of view image showing the fine structure of the cholesterol (*m/z* 369) within this feature, using an ion dose of 1.2×10^{11} ions/cm^2.

liquid metal ion sources (LMIS), and this is demonstrated in Fig. 5, where an area of rat brain tissue is imaged using a 40 keV C_{60}^+ beam.

The images (a–d) are from a 800 μm × 800 μm area that illustrates the interface between the corpus callosum feature (white matter) and the predominantly phospholipid dominated grey matter. The images clearly show the difference in chemistry between the white and grey matter. The cholesterol (*m/z* 369; Fig. 5c) is confined to the white matter, whilst the subsequent images, the collection of phospholipid quasi-molecular ion peaks at *m/z* 700–850 (Fig. 5b), the PC headgroup *m/z* 184 (Fig. 5a), and a single phospholipid quasi-molecular ion at *m/z* 760 (Fig. 5d) all demonstrate chemistry that is characteristic to the grey matter. Image (Fig. 5e) is a 200 μm × 200 μm area of the boundary between the white and grey matter, where the fine structure of the cholesterol (based on the *m/z* 369 ion) is clearly visible, with features with a diameter of 25 μm readily distinguishable.

3.4. Drug molecule imaging from in vivo studies

The high ion detection efficiency and improved imaging capabilities demonstrated in the previous sections indicate that conditions are now suitable to allow the distribution of compounds of markedly lower concentrations to be imaged, and not only the abundant native molecules. Fig. 6 shows the mapping of the drug raclopride within a section of rat brain containing the striatum from an animal dosed with the drug in vivo. The estimated concentration of the drug in the bulk organ is in the region of 2 ppm as determined by ESI-MS (S. Summerfield, GSK, Harlow, personal communication). Raclopride is a molecule that specifically binds to dopamine-D2 receptors within the brain, and a ^{11}C containing variant is commonly used in positron emission tomography to map the location of these receptors [31]. The selected ion images shown in Fig. 6a–c relate to the shaded area of the optical image in Fig. 6d. In order to identify the different domains within the section, the distribution of the PC headgroup ion at *m/z* 184 (Fig. 6a) and cholesterol ion, *m/z* 369 (Fig. 6b), are shown. From the accompanying spectrum, peaks relating to the $[M+H]^+$ of the drug raclopride are clearly visible to the left of a cluster of peaks relating to a cholesterol fragments within the drug containing section and absent from a representative control section spectrum. The distribution of this peak was then imaged using the C_{60}^+ ion beam and presented in Fig. 6c. However, the distribution demonstrated by the SIMS analysis does not accurately corroborate with the known locations of D2 receptor sites [32]. These data, whilst encouraging with respect to detection levels, offers two possible explanations for the result obtained, both of which involve common challenges encountered with SIMS and other mass spectrometry analysis. One possible explanation is that there is redistribution of the drug within the sample on entering the vacuum. It has been shown that cholesterol migration at room temperature can yield different results from the same tissue section depending on the temperature the sample is

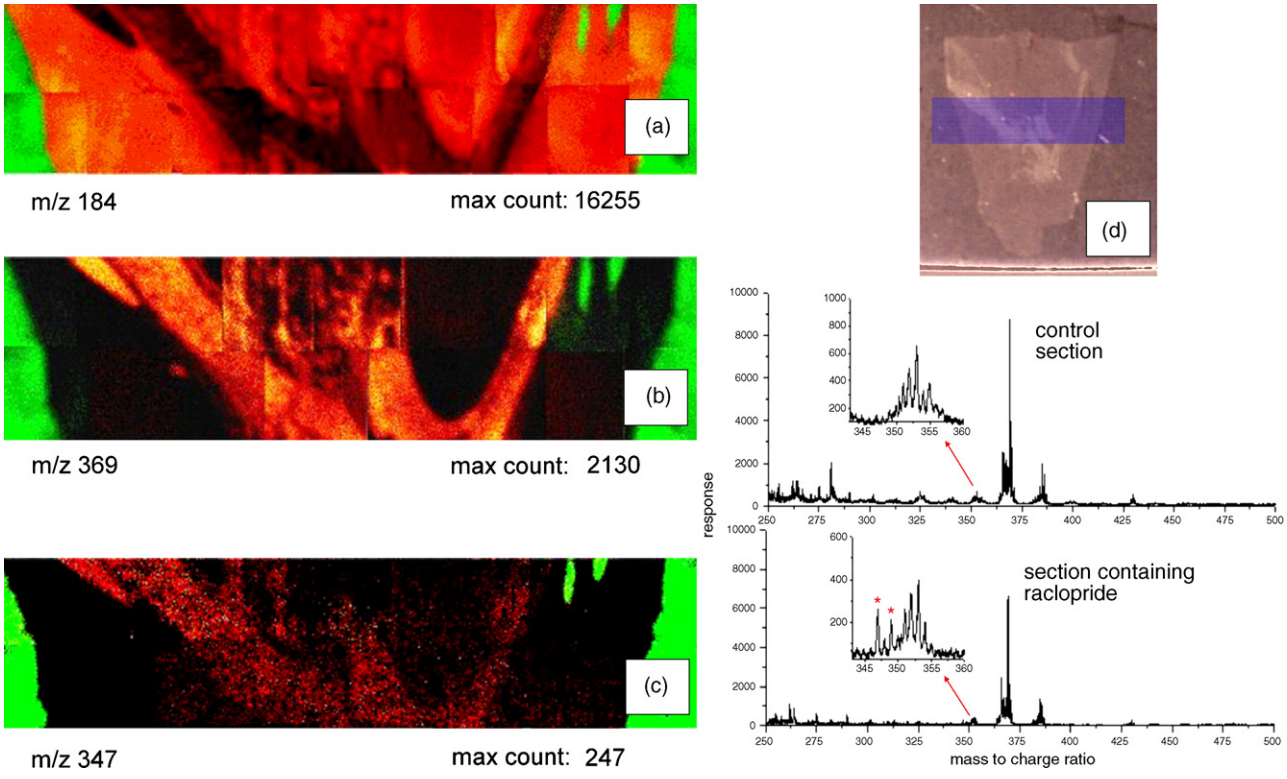

Fig. 6. A SIMS imaging investigation into the distribution of the drug raclopride from a section taken from a rat dosed in vivo. In the inset mass spectra, the lower spectrum demonstrates the presence of the $[M+H]^+$ of the raclopride at *m/z* 347 with its isotope peak at *m/z* 349, which are absent from the control spectrum. The images are shown on a thermal scale and illustrate the distribution of: (a) *m/z* 184 from phosphatidylcholine headgroup, (b) *m/z* 369 from cholesterol and (c) *m/z* 347 from the drug raclopride, the maximum counts per pixel of the ion of interest are quoted. In all of the images, the green pixels represent the substrate. The optical image (d) shows the area that was analysed. The total imaged area was 1.6 mm × 8.0 mm, with an ion dose of 8.8×10^{11} ion/cm^2.

held at during analysis [33], although there is much more to be understood of the mechanisms behind this molecular movement. The other possible cause is a familiar problem within dynamic SIMS, but not so frequently highlighted for organic SIMS, *the matrix effect*. It is to be noted from Fig. 6c that the $[M+H]^+$ signal from the drug closely resembles the distribution of cholesterol (Fig. 6b) which is indicative of the myelin rich white matter of the brain. It has previously been shown that cholesterol can provide a chemical environment that promotes the protonation of a species, whilst the phosphatidylcholine containing lipids act to suppress the $[M+H]^+$ signal from a typical drug compound [34].

3.5. Matrix effects

In order to investigate whether a matrix effect could explain the results in Fig. 6, a control section of rat brain was spin coated with 5 μL of a 1×10^{-3} M concentration solution of a related drug molecule (haloperidol) which should provide a sub-monolayer covering of the drug over the surface. When the tissue section was imaged there were significant similarities to the raclopride result in Fig. 6. In Fig. 7, the distribution of drug $[M+H]^+$ signal (*m/z* 376) across two different domains of the tissue is shown. The signal from the PC headgroup (*m/z* 184) indicates the distribution of grey matter, whilst the peak from the cholesterol (*m/z* 369) is again used to demonstrate the localisation of white matter. The same areas in both the 'real world' and model examples were also analysed in the negative polarity in order to investigate whether the distribution of the drug based on the $[M-H]^-$ ion could be compared to that of the $[M+H]^+$. However, no quasi-molecular or characteristic fragment ions could be detected, which is in keeping with the data from analysis of pure films of these drugs where the positive ions are heavily favoured due to the basic nature of the molecules. This model system demonstrates the severity of the suppression/enhancement effects that can be encountered across a two-domain system such as brain tissue sections. Without prior knowledge of the system in question it would be easy to assume that the peak at *m/z* 376 was linked to the constituents of the white matter along with the cholesterol.

Matrix effects are a common problem within analytical science and well known in mass spectrometry. High salt concentrations have been identified as interfering with electrospray ionisation mass spectrometry (ESI) analyses [35] as well as with MALDI [36,37], whilst the effects of physiological compounds in suppressing ionisation has also been reported in ESI [38]. The implication of this for SIMS of biological tissue is that great care must be taken interpreting the results of an analysis, and that full quantitative data may not be possible, as factoring for the effects of different chemical domains may need to be incorporated into the data handling.

One possible route to overcoming the matrix effect is to probe the high yield of sputtered neutrals using laser post-ionisation [39]. Although much has been made of the use of post-ionisation (PI) methods to increase the yields within SIMS experiments, the complexity of the experiment and the large differences in the success of the experiment depending upon the molecule of interest has seen the technique largely neglected recently, especially for obtaining molecular information. To test this possibility we prepared a model sample consisting of the drug atropine in 1:1 mixtures with both cholesterol and DPPC. The samples were analysed using C_{60}^+ SIMS in the conventional manner and laser post-ionisation of the sputtered neutrals. The results presented in Fig. 8 clearly show a great difference in the intensity of the drug molecule within the SIMS experiment, with the intensity of the $[M+H]^+$ at *m/z* 290 and major fragment at *m/z* 124 differing by an order of magnitude between the two lipid matrices. When the same samples are analysed using laser post-ionisation the most abundant representative ion seen from the drug is the fragment peak at *m/z* 124, the $[M+H]^+$ ion of course is not generated by laser PI. When the intensity of this peak is compared across the two samples the difference is negligible within experimental error. This suggests that the same amount of the drug molecule is present at the surface to be sampled, and the same number are being sputtered into the vacuum, however the nature of the sample has a great effect upon the percentage of these molecules that enter the vacuum in a charged state.

As well as being a method for illustrating the severity of the matrix effects that may be encountered within biological samples, this experiment also highlights the potential benefits of separating the desorption and ionisation steps within surface mass spectrometry.

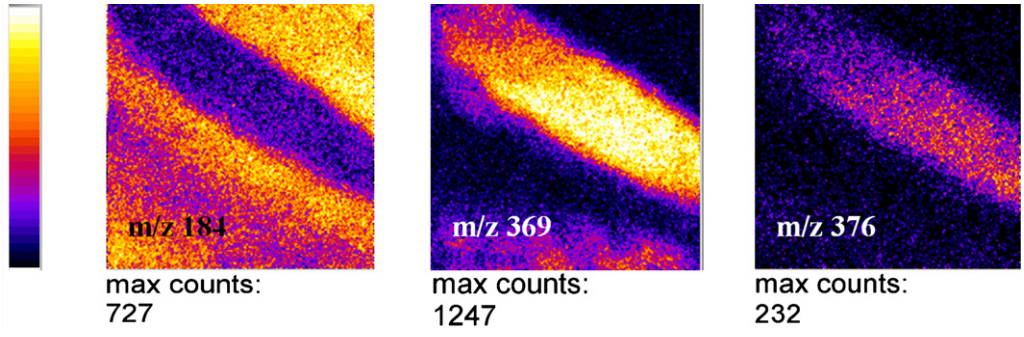

Fig. 7. Distribution of the molecular signal of the drug haloperidol ($[M+H]^+$ signal at *m/z* 376) spun cast onto a section of brain with respect to the chemical domains of the tissue. The signal from cholesterol (*m/z* 369) and phosphatidylcholine (*m/z* 184) are shown to indicate the different chemical domains within the tissue surface; the analysed area is 800 μm × 800 μm with a dose of 8×10^{10} ion/cm^2. Although the drug species covered the whole area visible in the image, the molecular signal is only detected from the cholesterol rich areas.

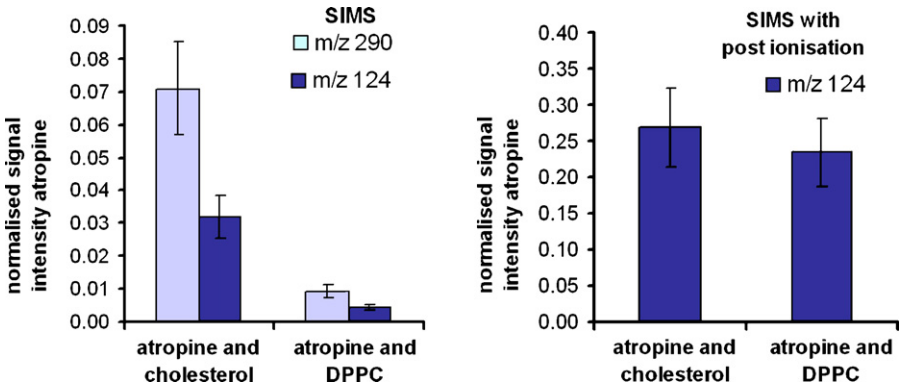

Fig. 8. The analysis of a drug molecule mixed with two abundant biological lipids, cholesterol and DPPC. The SIMS analysis, reliant upon ionisation at or just above the surface demonstrates strong differences between the ionisation probability of the drug atropine to its $[M+H]^+$ ion (*m/z* 290) and major fragment (*m/z* 124), whereas when the molecule is laser post-ionised the difference is negligible within experimental error. The ion used to identify the atropine in the laser post-ionisation was a characteristic fragment at *m/z* 124.

4. Discussion/conclusion

From the data presented here it is clear that the C_{60}^+ primary ion can make a great contribution to biological imaging, especially with the new generation ion beam technology that provides higher primary ion energies, fluxes and spot focussing. However, for molecular imaging of surfaces the secondary ion yields and minimum spot size only describe part of the requirements for effective imaging. With decreasing pixel sizes the number of ions available for sampling decreases accordingly. With the problem of bombardment-induced damage this issue begins to become the dominant factor for sub-micron resolution imaging. The plot in Fig. 9 shows how the number of molecular secondary ions that may expected from a given pixel area varies as a function of the ion detection efficiency based on the data for cholesterol collected for Table 2. The C_{60}^+ efficiency value in italics is that calculated using the disappearance cross-section from the steady state as discussed previously. The plot shows that the efficiency of Au^+ and Bi^+ bombardment on the tissue

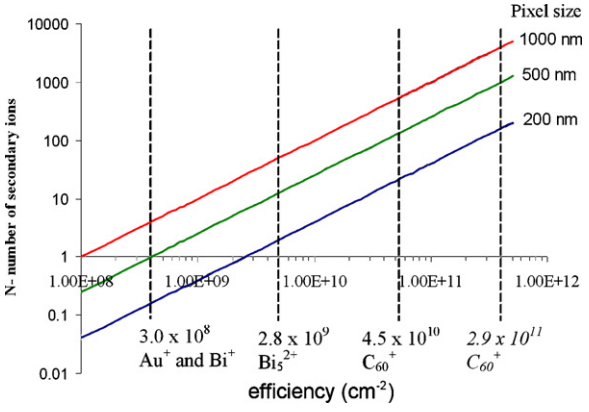

Fig. 9. A plot demonstrating the number of secondary ions of a given species (the *m/z* 385 ion from cholesterol in this case) that are theoretically available from a given pixel size as a function of secondary ion detection efficiency. The vertical lines have been added to illustrate the efficiencies calculated for the monatomic ions Au^+ and Bi^+, the cluster ion Bi_5^{2+} and C_{60}^+. The two values for C_{60}^+ represent the efficiency calculated from the average disappearance cross-section and then the disappearance cross-section at the steady state.

section is so low as to mean that it is improbable that a secondary ion yield >1 will be obtained from a 500 nm pixel, even though the beam can easily be focussed to provide this spatial resolution. It is only when the efficiencies of polyatomic ion beams are placed onto the plot that useful secondary ion yields are obtained.

Whilst the above conclusion is undoubtedly true, some qualification is required. It should be borne in mind that a *static SIMS* mode of thinking has been used to define the *detection efficiency* in terms of the *disappearance cross-section.* The disappearance cross-section as determined above in Section 3.1 assumes that the main contributor to the decay of the secondary ion signal will be ion bombardment-induced destruction of the surface chemistry. If damage accumulation is close to zero, then the only contributor to the disappearance cross-section would be removal of molecules. However, for multilayer samples the secondary ion signal will not reflect this loss until the sample remaining is less than the information depth of the primary ion, i.e., around a few monolayers. Thus, for thick samples disappearance cross-sections of close to zero are in principle possible. This would result in efficiencies of close to infinity which would be meaningless. Fundamentally SI detection efficiency is defined as the probability that a sputtered molecule is transformed into a SI multiplied by the instrument transmission and detection efficiency for the ion:

$$E(X_i^+) = P(M \rightarrow X_i^+)T(X_i^+)D(X_i^+) \quad (3)$$

For such samples efficiency should be defined as SI yield $\times N_{PI}$ to sputter all analyte per unit area or volume.

$$E(X_i^+) = \frac{Y(X_i^+)\theta(M)}{Y_{C_{60}}(M^{tot})} \quad (4)$$

where $\theta(M)$ is the surface coverage of M and $Y_{C_{60}}(M^{tot})$ is the total sputter yield of M under C_{60} bombardment. The problem is that to determine this we need sputter yields. These can only be determined by measuring weight or volume lost from pure systems and there are very few measurements at present. If we take the C_{60} case in Table 2 with the steady state disappearance cross-section of 3×10^{-15} cm^2, this would

yield an efficiency of 5×10^{11} cm^{-2} or 50 ions (100 nm)$^{-2}$. However, the few measurements made so far suggest that the sputter yield of cholesterol will be >100 under C_{60} bombardment [40]. Assuming $\theta(M) \sim 4 \times 10^{14}$ mol/cm^2, then $\sim 4 \times 10^{12}$ C_{60} impacts would sputter 1 cm^2 of pure cholesterol, yielding a two-dimensional efficiency of 6×10^9 cm^{-2} or 0.6 ions (100 nm)$^{-2}$. Yields above this would require the removal of a number of layers resulting in *voxel* analysis. C_{60} can do this because it generates little damage. On this basis a *voxel* of (100 nm)^3 could deliver >100 ions enabling reasonable three-dimensional chemical speciation. However, the ion yield is still only 10^{-5} to 10^{-4}. If this could be raised there are very exciting possibilities for even better volume resolution.

It has also been demonstrated here that the signal from drug molecules within model biological systems showed negligible signal disappearance with C_{60}^+, and hence would have a two-dimensional efficiency theoretically approaching infinity. Voxel analysis would be possible in this case and the number of secondary ions that could be collected would be limited only by the thickness of the sample (assuming homogeneity) and the time taken to acquire the data.

Data collection rates are slow with the pulsed systems currently in use, especially with polyatomic ion beams as they either make up a relatively small percentage of the total ion current as in Bi and especially the Au:Ge sources, or have low total currents. With a different design of instrument, allowing much larger doses to be used whilst still collecting a large percentage of the ions created then SIMS imaging can be moved away from the traditional pixel paradigm, and introducing a more information rich voxel concept.

Despite this increase in available data there are still a number of challenges to fully realise the potential of SIMS analysis of biological systems. Even with the yield increases provided by C_{60}, ionisation probabilities are still very low and there is a great deal to be gained from improvements. The matrix effects discussed here could also provide significant challenges, especially for quantitative studies, which would certainly interest those in the field of drug discovery. It is clear that methods of controlling and enhancing the ionisation process are required. This work has demonstrated that laser PI can contribute in particular cases. A recent study from this laboratory has shown that where frozen water is the host matrix, cluster ion bombardment generates large quantities of protons that greatly enhance the yield of M + H ions from solute amino acids and nucleic bases [41]. We need to increase our understanding of the mechanisms involved, to enable us to develop methods to control and enhance ionisation, be it through altering the surface chemistry via matrix addition or pre-etching with a polyatomic ion beam; or de-coupling the desorption and ionisation steps through post-ionisation methods.

Acknowledgements

Financial support from the Engineering and Physical Sciences Research Council (EPSRC) and the Biotechnology and Biological Sciences Research Council (BBSRC) is gratefully acknowledged. From GlaxoSmithKline, Harlow, Scott Summerfield and Martin Vigeon-Hart are warmly thanked for their assistance by preparing and providing samples and Andy Organ, Frank Paul and Hayley Cordingley for sharing their expertise and knowledge.

References

[1] R. Levi-Setti, J.M. Chabala, K. Gavrilov, R. Espinosa III, M.M. Le Beau, Microsc. Res. Technol. 36 (1997) 301.
[2] J. Clerc, C. Fourré, P. Fragu, Cell Biol. Int. 21 (1997) 619.
[3] D.R. Lorey II., G.H. Morrison, S. Chandra, Anal. Chem. 73 (2001) 3947.
[4] E. Larra-Regard, M.-C. Mony, Int. J. Mass Spectrom. Ion Process. 143 (1995) 147.
[5] P.J. Todd, T.G. Schaaff, P. Chaurand, R.M. Caprioli, J. Mass Spectrom. 36 (2001) 355.
[6] P. Chaurand, R.M. Caprioli, Electrophoresis 23 (2002) 3125.
[7] B. Spengler, M. Hubert, J. Am. Soc. Mass Spectrom. 13 (2002) 735.
[8] S.A. Schwartz, M.L. Reyzer, R.M. Caprioli, J. Mass Spectrom. 38 (2003) 699.
[9] K. Dreisewerd, M. Schiirenberg, M. Karas, F. Hillenkamp, Int. J. Mass Spectrom. Ion Process. 141 (1995) 127.
[10] J.C. Vickerman, D. Briggs (Eds.), ToF-SIMS: Surface Analysis by Mass Spectrometry, IM Publications and Surface Spectra Limited, Charlton, Chichister, West Sussex, UK, 2001.
[11] N. Davis, D.E. Weibel, P. Blenkinsopp, N. Lockyer, R. Hill, J.C. Vickerman, Appl. Surf. Sci. 203–204 (2003) 223.
[12] F. Kollmer, Appl. Surf. Sci. 231–232 (2004) 153.
[13] D. Touboul, F. Kollmer, E. Niehuis, A. Brunelle, O. Laprevote, J. Am. Soc. Mass Spectrom. 16 (2005) 1608.
[14] D.E. Weibel, S. Wong, N.P. Lockyer, P. Blenkinsopp, R. Hill, J.C. Vickerman, Anal. Chem. 75 (2003) 1754.
[15] J. Cheng, N. Winograd, Anal. Chem. 77 (2005) 3651.
[16] C.M. Mahoney, S.V. Robertson, G. Gillen, Anal. Chem. 76 (2004) 3199.
[17] Z. Postawa, B. Czerwinski, M. Szewczyk, E.J. Smiley, N. Winograd, B.J. Garrison, J. Phys. Chem. B 108 (2004) 7831.
[18] Z. Postawa, B. Czerwinski, N. Winograd, B.J. Garrison, J. Phys. Chem. B 109 (2005) 11973.
[19] J. Fletcher, N.P. Lockyer, J.C. Vickerman Surf. Interface Anal., in press.
[20] Z. Takas, J.M. Wiseman, B. Gologan, R.G. Cooks, Science 306 (2004) 471.
[21] J. Shiea, M.-Z. Huang, H.-J. Hsu, C.-Y. Lee, C.-H. Yuan, I. Beech, J. Sunner, Rapid Commun. Mass Spectrom. 19 (2005) 3701.
[22] P. Sjövall, J. Lausmaa, B. Johansson, Anal. Chem. 76 (2004) 4271.
[23] T.M. Annesley, Clin. Chem. 49 (2003) 1041.
[24] R.M. Braun, P. Blenkinsopp, S.J. Mullock, C. Corlett, K.F. Willey, J.C. Vickerman, N. Winograd, Rapid Commun. Mass Spectrom. 12 (1998) 1246.
[25] D. Touboul, F. Halgand, A. Brunelle, R. Kersting, E. Tallarek, B. Hagenhoff, O. Laprevote, Anal. Chem. 76 (2004) 1550.
[26] H. Nygren, K. Börner, B. Hagenhoff, P. Malmberg, J.-E. Mansson, Biochim. Biophys. Acta 1737 (2005) 102.
[27] L.A. McDonnell, S.R. Piersma, A.F.M. Altelaar, T.H. Mize, S.L. Luxembourg, P.D.E.M. Verhaert, J. van Minnen, R.M.A. Heeren, J. Mass Spectrom. 40 (2005) 160.
[28] A.F.M. Altelaar, I. Klinkert, K. Jalink, R.P.J. de Lange, R.A.H. Adan, R.M.A. Heeren, S.R. Piersma, Anal. Chem. 78 (2006) 734.
[29] S.G. Ostrowski, C. Szakal, J. Kozole, T.P. Roddy, J. Xu, A.G. Ewing, N. Winograd, Anal. Chem. 77 (2005) 6190.
[30] M.F. Russo Jr., I.A. Wojciechowski, B.J. Garrison, Appl. Surf. Sci. 252 (2006) 6423.
[31] L. Farde, H. Hall, E. Ehrin, G. Sedvall, Science 231 (1986) 258.
[32] M. Camps, R. Cortes, B. Gueye, A. Probst, J.M. Palacios, Neuroscience 28 (1989) 275.
[33] P. Sjövall, B. Johansson, J. Lausmaa, Appl. Surf. Sci. 252 (2006) 6966.

[34] E.A. Jones, N.P. Lockyer, J.C. Vickerman, Appl. Surf. Sci. 252 (2006) 6727.
[35] L. Tang, P. Kebarle, Anal. Chem. 63 (1991) 2709.
[36] R. Kratzer, C. Eckerskorn, M. Karas, F. Lottspeich, Electrophoresis 19 (1998) 1910.
[37] F.M.L. Amado, P. Domingues, M. Graca Santana-Marques, A.J. Ferrer-Correia, K.B. Tomer, Rapid Commun. Mass Spectrom. 11 (1997) 1347.
[38] R. King, R. Bonfiglio, C. Fernandez-Metzler, C. Miller-Stein, T. Olah, J. Am. Soc. Mass spectrum. 11 (2000) 942.
[39] K.F. Willey, V. Vorsa, R.M. Braun, N. Winograd, Rapid Commun. Mass Spectrom. 12 (1998) 1253.
[40] J. Cheng, N. Winograd, Anal. Chem. 77 (2005) 3651.
[41] X.A. Conlan, N.P. Lockyer, J.C. Vickerman, Rapid Commun. Mass Spectrom. 20 (2006) 1327.